UNIVERSIDADE DE SÃO PAULO

INSTITUTO DE FÍSICA
CAIXA POSTAL 20516
01452-990 SÃO PAULO - SP
BRASIL

PUBLICAÇÕES

IFUSP/P-1101

MODELING MINI-ORANGE ELECTRON SPECTROMETERS

Nelson Canzian da Silva and **Olácio Dietzsch**
Instituto de Física, Universidade de São Paulo

Março/1994

Modeling mini-orange electron spectrometers

Nelson Canzian da Silva and Olacio Dietzsch

Instituto de Física, Universidade de São Paulo
C.P. 20516, São Paulo, SP 01498-970, Brazil

ABSTRACT

A method for calculating the transmission of mini-orange electron spectrometers is presented. The method makes use of the analytical solution for the magnetic field of a plane magnet in the calculation of the spectrometer spatial field distribution by superimposing the fields of the several magnets that compose the system. Electron trajectories through the spectrometer are integrated numerically in a Monte Carlo calculation and the transmission of the spectrometer as a function of the electron energy is evaluated. A six-magnet mini-orange spectrometer was built and its transmission functions for several distances from source to detector were measured and compared to the calculations. The overall agreement is found to be good. The method is quite general and can be applied to the design of systems composed of plane magnets, predicting their performance before assembling them.

Accepted for publication at
Nuclear Instruments and Methods in Physics Research
Section A

1 INTRODUCTION

The development of mini-orange (MO) electron spectrometers began in the 1970's [1] with the introduction of new magnetic materials capable of producing relatively intense fields with small quantities of bulk material. Since then, they have been systematically studied [2, 3, 4, 5, 6, 7] and applied to many experiments, such as spin and parity assignments of nuclear states [8], determination of the multipolarity of prompt transitions [9], and relative measurements of the longitudinal polarization of positrons and electrons [10], among others. Mini-orange spectrometers are small, light and versatile systems that offer a good background reduction for photons and low-energy charged particles, and can be designed in order to optimize acceptance for the desired electron energy interval.

Mini-orange spectrometers are made of small permanent magnets, usually rare-earth compounds (e.g., NdFeB, $SmCo_5$), placed as the sections of an orange, surrounding a central absorber. Fig. 1 presents the particular configuration used in the present work. A set of magnets and an absorber are placed between the source (or the target, in the case of experiments with accelerators) and the detector, usually a solid state one. The system acts as a lens and a filter: the magnetic field directs charged particles towards or away from the detector, depending on their charges, while the central absorber shades it from neutral (photons) radiation.

A MO spectrometer is characterized by its transmission, which may be defined as the ratio of the number of detected particles to the number of particles emitted by the source, per unit time. The transmission depends on the energy of the particle, on the magnetic field of the MO, and on the relative positions of source and detector. The magnetic field spatial distribution depends on the number and shape of the magnets, as well as on their magnetization. Although shapes and materials can vary, two basic magnet shapes are commonly used: plane and wedge-shaped.

Several attempts were made to describe the response of MO spectrometers. For

systems making use of wedge-shaped magnets, the approximation usually adopted [1, 8, 11, 12] is that of a homogenous toroidal field throughout the MO. In this way, the charged particles paths are straight lines out of the field and arc segments of constant radius inside it. This approach gives transmission curves with shapes similar to those obtained experimentally, but with much higher values, sometimes off by almost an order of magnitude. Dresel *et. al* [6] obtained good results for wedge-shaped magnet systems when a functional dependence of the field strength with the radial position was included. Later [7] they extended the method for fewer-magnet systems, which have more inhomogeneous fields. The method requires, however, field measurements at several regions of the gaps for every chosen configuration.

For plane-magnet systems, the toroidal field approximation does not work very well. The usual approach is to use extensive measurements of the field in the gaps of the MO and to numerically integrate the trajectories of the particles from source to detector. The quality of the results are usually similar or worse than those obtained for systems with wedge-shaped magnets.

In this work we present a method for the calculation of the transmission for systems made of plane magnets. The field is calculated from the analytical solution of the Maxwell equations for the field of a single thin plane rectangular magnet. The superposition of the fields created by all the magnets in the MO gives the total field. We follow the method of Wu and Armstrong [14] to describe the magnetic field produced by a system made of two plane magnets. The path of the particles through the system is integrated numerically. Only partial measurements of the magnetic field of individual magnets are necessary to adjust the analytical solution and, once it is done, the resultant field can be calculated for any configuration of the magnets.

The method presented here should therefore be useful in reliably predicting the transmission functions of MO spectrometers based on assemblies of plane magnets in any geometrical configuration without having to perform a detailed mapping of the magnetic field of the assembled systems.

2 METHOD OF CALCULATION

2.1 Magnetic Field of a Single Magnet

For a thin plane rectangular magnet, as shown in fig. 2, with uniform magnetization vector $\vec{M}(\vec{r})$ perpendicular to its larger face, the Maxwell equations can be integrated analytically, without further approximations. The induction vector $\vec{B}(\vec{r})$ produced by a medium with magnetization $\vec{M}(\vec{r})$ is given by [13]:

$$\vec{B}(\vec{r}) = \frac{1}{c}\int_V \rho_M(\vec{r}')\frac{(\vec{r}-\vec{r}')}{|\vec{r}-\vec{r}'|^3}dv' + \frac{1}{c}\int_S \sigma_M(\vec{r}')\frac{(\vec{r}-\vec{r}')}{|\vec{r}-\vec{r}'|^3}da', \tag{1}$$

where $\rho_M(\vec{r}') = -\nabla(\vec{r}')\cdot\vec{M}(\vec{r})$ and $\sigma_M(\vec{r}') = \vec{M}(\vec{r})\cdot\vec{n}$ are the volume and surface magnetization densities. If $\vec{M}(\vec{r}) = M_0\hat{z}$, then $\rho_M(\vec{r}') = 0$ and $\sigma_M(\vec{r}') = M_0$. Thus, the induction vector becomes

$$\vec{B}(\vec{r}) = \frac{M_0}{c}\int_S \frac{(\vec{r}-\vec{r}')}{|\vec{r}-\vec{r}'|^3}da'. \tag{2}$$

Adopting the coordinate system of fig. 2, with origin at the center of the magnet (length 2ℓ and width $2a$), the integration of eq. 2 gives [14], for each component of $\vec{B}(\vec{r})$,

$$B_x(x,y,z) = \frac{M_0}{c} \times \ln \frac{(y-a)+\sqrt{(x+l)^2+(y-a)^2+z^2}}{(y+a)+\sqrt{(x-l)^2+(y+a)^2+z^2}} \times$$
$$\frac{(y+a)+\sqrt{(x-l)^2+(y+a)^2+z^2}}{(y-a)+\sqrt{(x-l)^2+(y-a)^2+z^2}},$$
$$B_y(x,y,z) = \frac{M_0}{c} \times \ln \frac{(x-l)+\sqrt{(x-l)^2+(y+a)^2+z^2}}{(x-l)+\sqrt{(x-l)^2+(y+a)^2+z^2}} \times$$
$$\frac{(x+l)+\sqrt{(x+l)^2+(y-a)^2+z^2}}{(x-l)+\sqrt{(x-l)^2+(y-a)^2+z^2}}, \tag{3}$$

$$B_z(x,y,z) = \frac{M_0}{c} \times \arctan\left(\frac{(x+l)(y+a)}{z\sqrt{(x+l)^2+(y+a)^2+z^2}}\right) -$$
$$\arctan\left(\frac{(x-l)(y+a)}{z\sqrt{(x-l)^2+(y+a)^2+z^2}}\right) -$$
$$\arctan\left(\frac{(x+l)(y-a)}{z\sqrt{(x+l)^2+(y-a)^2+z^2}}\right) +$$
$$\arctan\left(\frac{(x-l)(y-a)}{z\sqrt{(x-l)^2+(y-a)^2+z^2}}\right).$$

In order to account for non-uniformities in the magnetization of different regions of the magnets, they are supposed to be made out of an arbitrary number of smaller rectangular "magnets". Each of these "partition magnets" has a constant magnetization. The field of the real magnet is calculated as the superposition of the fields produced by the smaller pieces. For this purpose, coordinate transformations are applied, which relate points in the magnet coordinate system to the partition coordinate system. The number and dimensions of the partition "magnets" used in the calculations reported here are shown schematically in fig. 2. Their magnetization will be discussed in Section 3.2.

2.2 Superposition of the Fields

The resultant magnetic field at any given point in the mini-orange spectrometer is evaluated by superimposing the fields of all magnets in that particular geometric configuration. The coordinates $\vec{r}_{MO} \equiv (x_{MO}, y_{MO}, z_{MO})$, of a given point described in the MO coordinate system, shown in fig. 3, have to undergo a set of rotations and translations in order to correspond to a point $\vec{r}_i \equiv (x_i, y_i, z_i)$ in each magnet coordinate system. Such rotations and translations take a magnet originally centered at the origin of the MO system to its respective position in the MO and can be written as:

$$\vec{r}_{MO} = \mathbf{R}_i \cdot (\mathbf{R}_C \cdot \vec{r}_i + \mathbf{T}), \qquad (4)$$

where $\mathbf{R}_C$ and $\mathbf{T}$ are the rotation and translation matrices, respectively, that define the orientation and position of one magnet with respect to the symmetry axis. $\mathbf{R}_i$ are rotations that are used to "transport" the magnets to their places in the mini-orange. The set of transformations used in the calculations for the particular configuration shown in fig. 1 is indicated in fig. 4.

Once the field is calculated for each magnet in its proper coordinate system, the components have to be transformed back to the MO coordinate system and superimposed according to:

$$\vec{B}_{MO}(\vec{r}) = \sum_{i=1}^{n} \mathbf{R}_i \cdot \mathbf{R}_C \cdot \vec{B}_i(\vec{r}_i), \qquad (5)$$

where the sum is carried over all the magnets in the system.

2.3 Integration of the Trajectories

The trajectories of relativistic electrons with energy E and mass m_0, subjected to the Lorentz force, are described by the equations of motion

$$\frac{dv_i}{dt} = -\frac{e}{mc}(v_j \cdot B_k - v_k \cdot B_j), \qquad (6)$$

where $m = m_0\gamma$ and $\gamma = 1 + E/m_0c^2$, and i, j and k are the indexes corresponding to the three spatial components.

Numerical techniques (the fourth order Runge-Kutta method [15]) were used to integrate equations (6). The method requires the values of the magnetic field at all points of space, the coordinates of the source – from where the electrons are emitted – and their initial velocity vector, obtained from their energy E and the emission angle (ϑ, φ). The coordinate system for the spectrometer and the parameters used in the calculations are shown in fig. 3. It is also necessary to specify the geometrical boundary conditions such as the central absorber, the magnets and their support structures, and the detector.

In the calculations, electrons in a given energy range were considered to be emitted from a point source in random directions contained in one half of a sector of the spec-

trometer. This corresponds to $1/12^{th}$ of the full solid angle. Electron trajectories are computed until the electron either: (*i*) hits the detector; (*ii*) passes through the MO but misses the detector; (*iii*) hits the surface of the magnets; (*iv*) hits the ring that supports the magnets; (*v*) is out of the range of the field, i.e., its radial coordinate is too large; or (*vi*) hits the central absorber.

The *end condition*, or the reason why the path integration is interrupted, is recorded for every trajectory in order to provide some insight about what happens to those electrons that do not hit the detector. For those electrons which hit the detector, the emission angles and final coordinates and velocities are also recorded. Electrons have a non-negligible probability of being backscattered at the surface of the detector. To evaluate the backscattering probability η, which is a function of the energy and angle of incidence, a semi-empirical formulation described in ref. [16] is used. The angle of incidence in the detector is calculated and the backscattering probability is computed and used as a weighting factor while filling the histograms.

3 MEASUREMENTS

3.1 Experimental Set-up

Fig. 5 presents the experimental set-up used in the measurements of the transmission functions. Three aluminum disks, one for holding the source, one for the MO and one for the detector, are supported by three non-magnetic metal rods. The three disks are free to slide along the rods. A scale is engraved in one of the rods, allowing a precise determination of the relative position of the components. The system is enclosed in a vacuum chamber and the measurements were done at a pressure of 10^{-6} Torr.

Sources of ^{133}Ba, ^{137}Cs and ^{207}Bi are used. They were made by Isotope Products Co., and consist of a mylar (or aluminized mylar) thin foil, over which a droplet of a solution containing the radioactive element has been deposited. The mylar foils are held by a ring

2.54 cm in diameter supported by one of the aluminum discs shown in fig. 5. Holding the source in place is a collimator with an aperture 5 mm in diameter. The detector is a fully depleted silicon surface barrier detector, with a nominal active area of 2.0 cm^2 and a thickness of 0.2 cm. An aluminum collimator with a circular aperture 1.6 cm in diameter was placed in front of the detector.

The MO spectrometer is also supported by an aluminum ring with fixtures to accommodate the magnets (six, in the configuration studied here) and to keep them simmetrically placed. The central absorber is a 4.0 cm long truncated double-conical piece of lead, 1.0 cm in diameter in its smaller radius and 2.0 cm in diameter in its larger radius. The magnets are plane rectangular pieces, 2.54 cm wide, 3.81 cm long and 0.32 cm thick, made of sinterized $SmCo_5$ powder, manufactured by Magnox Inc. They are placed tilted at an angle of 45° with respect to the symmetry axis, with one of their corners resting in the wedge-shaped recess of the absorber.

Standard electronic circuits were used for the measurements, with pre-amplifier and amplifier stages followed either by a multi-channel analyzer or by a CAMAC based data acquisition system connected to a computer. The measurements were made at room temperature. The experimental energy resolution (FWHM) was 15 keV.

3.2 Magnetic Field Measurements

In order to calculate the transmission function, knowledge of the magnetic field is essential. In the approach adopted here there is no need to map the field of the MO itself. Information about the fields of the individual magnets, which are easier to get experimentally, are used instead.

The magnetic field distribution associated with each face of individual magnets was measured with a Hall probe running along the x and y axes (fig. 2) of the magnet, at different distances (z) from the surface. The area of the sensing element was about

0.1 cm^2, and the measurements were taken in each direction at points 0.4 cm apart. A precision $X - Y$ motor-driven table was used, and the position of the magnet or of the Hall probe could be modified and recorded by a computer. The measured values of the magnetic field were also digitized and recorded by the system.

Magnetic field measurements in the space above the larger faces of eight similar magnets showed differences of up to 20% from magnet to magnet. Differences between the fields at the two large faces of the same magnet were also detected. Fig. 6 presents a set of measurements (dashed lines) for one magnet, along the x and y axes (cf. fig. 2), at planes parallel to the face of the magnet, corresponding to different values of z.

It is apparent from fig. 6 that near the surface of the magnet (i.e., for low values of z), the field is stronger over the edges of the magnet than at its center. In order to reproduce this behavior in the calculations, each magnet was treated as five smaller rectangular pieces (partitions), shown by dashed lines in fig. 2. The central piece was assigned a magnetization M_c and the four peripheral pieces a magnetization $M_p = f_M \cdot M_c$. The partition dimensions, defined by p and q as shown in fig. 2, as well as the magnetization M_c and the proportionality factor f_M were treated as adjustable parameters in fitting the experimental data for the magnetic field.

The values of the parameters were chosen to minimize the average squared deviation (weighted by the inverse square of the experimental uncertainty) between measured and calculated values. The dimensions of the partition pieces were the same for all magnets, $p = 0.33a$ and $q = 0.25\ell$, where ℓ and a are the length and the width of the magnets, respectively. The factor $f_M = 1.4$ was also taken to be the same for all magnets. The magnetization constant M_c assumed values from 150 to 190 Gauss, depending on the magnet. M_c was treated as an independent parameter in fitting data for the x and y directions, with data at all z planes being included in the calculation of the average deviations. Fig. 6 shows the result (solid lines) of the the analytical solution for the field,

calculated with a set of parameters obtained as described above.

Good fits were obtained only when a positive constant was subtracted from the calculated field values. Though physically inconsistent with the fact that the solution should go to zero at large distances, this constant can be interpreted as a correction for the effect of the finite thickness of the magnet and a non-zero volumetric magnetization density. As such, it is an approximation to the value of the first integral in eq. 1. For symmetry reasons, however, the effect of this constant disappears when the field of the individual magnets are superimposed to build up the total field of the mini-orange.

Magnetic field distributions with approximately the same magnitude at corresponding points in all gaps of a MO spectrometer can considerably simplify the transmission calculations. For then, the trajectory integrations can be done for just half of a gap of the MO and the result multiplied by twice the number of gaps. A procedure was thus devised in order to choose six out of eight otherwise similar magnets, as well as their relative positions in the MO, so as to produce approximately equal fields in all gaps of the assembled MO.

For this procedure, parameters were extracted from the field measurements of the individual magnets, which would characterize the intensity of the field at each face of each magnet, such as the value of the field at the center of the face or the average of the measurements along the axes. Using these parameters, and given the relative positions of the magnets in the MO, "average" fields of each gap and of the MO as a whole were calculated. The associated standard deviation was used as a measure of the homogeneity of the field of the MO. The experimental MO set-up used in the measurements was built with the six magnets positioned according to the order and face orientation found for the configuration with the lowest standard deviation. The average value of M_c found for the six magnets in this configuration, 171$\pm$6 Gauss, was adopted in the MO transmission calculation procedure.

3.3 Transmission Function Measurements

The transmission function can be expressed as a function of the MO parameters, as:

$$T(E,\mathcal{C}) = \frac{A(E,\mathcal{C})}{A_0(E)}, \tag{7}$$

where $A_0(E)$ is the total number of electrons of energy E emitted by the source over the full 4π solid angle, per unit time. $A(E,\mathcal{C})$ is the number of electrons collected by the detector with the spectrometer in the configuration $\mathcal{C} \equiv \{f, g, \vec{B}\}$, that refers to the particular combination of source to MO distance (f) and detector to MO distance (g), and to the field distribution $\vec{B}$, which is determined by the the number, shape, position and magnetization of the magnets.

Transmission measurements were made for conversion electron lines of nine different energies, ranging from 265 keV to 1047 keV, as specified in table 1. For all energies, measurements were made for 6 different combinations of the source-MO (f =3.7, 4.2, 4.7 cm) and detector-MO (g =1.9, 2.9 cm) separations. The coordinate system is the same one used in the calculations, shown in fig. 3.

The evaluation of the transmission requires the knowledge of the total emissivity of the source for each conversion line. Source intensity measurements were performed with the same set-up, but without the MO and its support structures. Intensity measurements were made for each electron energy at several distances r_{SD} from source to detector. The number of electrons $A(E, r_{SD})$ collected by the detector (with an active area S_D) can be written as a function of the total number of electrons $A_0(E)$ emitted by the source, the backscattering probability $\eta(E,\theta')$ and the solid angle $d\Omega \simeq S_D/r_{SD}^2$, as:

$$A(E, r_{SD}) \simeq \frac{1}{4\pi} \cdot A_0(E) \cdot (1-\eta) \cdot \frac{S_D}{r_{SD}^2}. \tag{8}$$

A straight line adjusted to the measurements of $A(E, r_{SD})$ vs. $1/r_{SD}^2$ allowed the determination of $A_0(E)$. The angle of incidence of the electrons onto the detector, for this situation, is close to 0°, and a backscattering probability of 0.15 was adopted [16]. The error in the determination of the absolute activity of the source comes primarily from the uncertainty in the backscattering probability, which is of the order of 10%.

4 RESULTS

Fig. 7 shows electron spectra taken with and without the mini-orange spectrometer of fig. 1. The normalization is such that the peak maximum for the 626 keV line of the ^{137}Cs source be the same in both cases. The effect of the spectrometer on the low energy part of the spectrum is clearly seen.

The measured and calculated transmission functions obtained in the present work are presented in fig. 8. The error bars of the experimental data are statistical uncertainties only. The uncertainty in the absolute values is estimated to be of the order of 15%, and comes essentially from the uncertainty in the determination of the absolute activity of the sources and in the measurement of distances and dimensions of the parts of the system. For the calculated values, the uncertainty comes mainly from that associated with the backscattering probability, which is of the order of 10%. The results of the calculations reproduce quite well the data in overall shape and magnitude for all geometrical configurations and electron energies. There are, however, a few discrepancies between the calculated and measured values, which are addressed below.

Fig. 9 shows the distribution of the azimuthal emission angles of the detected electrons, for two different energies and configurations, as given by the calculation. This sample is representative of the general shapes of distributions for all energies and configurations. The main feature in all cases is that only electrons emitted towards the central region of the gap ($|\vartheta_{max}| < 15°$) are eventually detected. For low energies the general trend is a maximum at the center of the gap, with the distribution falling slowly with an increasing $|\vartheta|$. As the energy increases a central plateau begins to take shape, with a

steeper fall-off and aperture endpoints lower than those found at lower energies.

The calculations also show that the distributions for the polar emission angle of the electrons that eventually reach the detector are usually very narrow, centered at an angle which is strongly dependent on the energy. Fig. 10 shows, for the six configurations studied, the mean value (φ_{ave}, scale at left) and the r.m.s. width ($\Delta\varphi_{rms}$, scale at right), indicating, as expected, that they are strongly dependent on the polar angle interval.

The electrons that do not reach the detector can also give some insight about the system. The majority of the low energy electrons admitted into the field region of the spectrometer (70% of the total emitted in $1/12^{th}$ of 4π) usually end up hitting the face of the magnets, or, in slightly lower fractions, being deflected towards the central absorber. At higher energies, fewer electrons hit the magnets or the absorber, and end up missing the detector.

The calculations give systematically lower values for the transmission at higher energies. This is a very sensitive situation, for results of both experiment and calculation depend strongly on the electron direction of motion and the geometry of the MO and therefore can be subject to large systematic errors. The paths of the more energetic electrons which are detected run very close to the surface of the central absorber so that the lower limit for the azimuthal emission angles of the detected electrons is usually given by the geometrical boundaries of the absorber. The upper limit of the intervals, on the other hand, is determined by those tracks which end up at the detector at its outermost part. Due to the small angular aperture ($< 1°$), small misalignments within the system or a small inaccuracy in the geometrical description in the simulation may lead to large changes in the measured and calculated values for the transmission.

The finite size of the source, which is not taken into account in the calculations, can be responsible for part of the discrepancies found mainly in the configurations with smaller distances from source to MO. The size of the source, about 0.5 cm in diameter,

is not negligible when compared to the distances from source to MO (typically 3-5 cm), considering that the distances to regions of appreciable fields are the smallest that the electron travels. This effect is enhanced by the small angular apertures involved.

5 CONCLUSION

The method presented here for the modeling of mini-orange electron spectrometers seems to be quite appropriate as a design tool for such systems. Prior to the construction of the spectrometer one can explore many possible choices of number, position, shape and magnetization of the magnets, as well as distances from source to MO, in order to decide which is the most suitable configuration for a particular purpose. The required computer power is well suited for processing in a table-top computer. The method, however, does not replace the need to measure the transmission function of the final configuration adopted in any experiment, the actual transmission being very sensitive to small experimental details. Furthermore, the calculation does not provide the accuracy usually required when correcting the data. The application of the method, very general in its principles, is not restricted to mini-orange spectrometers, being easily adaptable to similar systems.

ACKNOWLEDGEMENTS

The help received from E. L. A. Macchione, Y. Miyao, J. Takahashi, K. Koide, R. Shimazaki and E. M. Takagui is gratefully acknowledged. We would like to thank the Magnet Group of the National Synchrotron Light Source (Campinas, São Paulo) for their help in the measurement of the magnetic fields. We would also like to thank the Omega Group of the Brookhaven National Laboratory for the warm hospitality extended to us at BNL where part of this work was carried out. One of us (OD) would like to acknowledge fruitful conversations over the years on this subject with J. X. Saladin, I. Y. Lee, M. P. Metlay and C. C. Kuo. This research was supported, in part, by the Financiadora de

Estudos e Projetos (FINEP), Conselho Nacional de Pesquisa e Desenvolvimento (CNPq) and Fundação de Amparo à Pesquisa do Estado de São Paulo (FAPESP).

TABLES

Table 1. Radioactive sources used in this work and their conversion e^- line energies (approximate values).

Isotope	Conversion e^- energy (keV)			
^{133}Ba	265	319	346	
^{137}Cs	626	656		
^{207}Bi	479	553	973	1047

LIST OF FIGURES

1. The mini-orange (MO) spectrometer used in the measurements reported in this work and for which calculations were performed. (1) conversion electron source; (2) lead absorber; (3) magnets; (4) surface barrier Si detector. An electron "track" through the MO is also shown. The diameter of the system is about 10 cm.

2. Magnet coordinate system adopted in the calculation of the field of a single magnet. Also shown by dashed lines is the "partition" scheme described in the text. For this work $p = 0.33a$ and $q = 0.25\ell$. The magnetization of the peripheral regions is taken as 1.4 times that of the central region (see text).

3. Mini-orange coordinate system. The distances from source to MO and detector to MO are represented by f and g, respectively. The polar emission angle φ is measured relative to the symmetry direction z. The azimuthal emission angle ϑ is measured in the xy plane.

4. Transformations relating the coordinate system of a single magnet to that of the MO. (a) the magnet in its own coordinate system; (b) after a 90° rotation around y; (c) after a 45° rotation around x'; (d) after a translation on the plane $x''y''$ and (e) after a 60° rotation around z'''.

5. Experimental setup. (1) Source holder; (2) magnet holder; (3) detector holder; (4) central lead absorber; (5) magnets; (6) sustaining rods. A scale is engraved in one of the rods to measure the distances between source, central absorber and detector.

6. Experimental (dashed lines) and calculated (solid lines) z component of the magnetic field above one of the larger faces of a single magnet. The measurements were taken along (a) the x-axis and (b) the y-axis of the magnet (see fig. 2), for $z = 6, 9, 13, 18, 24$ mm. Calculated curves (see text) are for the same z values. The vertical arrows indicate the edges of the magnet.

7. Electron spectra, taken with a ^{137}Cs source, with and without the mini-orange spectrometer. Intensities were normalized to the 626 keV peaks to show the effect of the MO on the low energy region.

8. Transmission of the mini-orange for different combinations of source to MO (f) and detector to MO (g) distances measured in cm (see fig. 3). Circles are experimental data, solid lines connect calculated values. The error bars are statistical uncertainties only.

9. Calculated distributions for the azimuthal emission angles of detected electrons for electron energies of 346 keV (solid lines) and 656 keV (dashed lines), for two sets of f and g distances (see fig. 3) given in cm.

10. Average value (φ_{ave}, scale at left) and aperture ($\Delta\varphi_{rms}$, scale at right) for the polar emission angle distribution for detected electrons. Distances f and g (see fig. 3) are given in cm.

References

[1] J. van Klinken and K. Wisshak, Nucl. Instr. and Meth., 98(1972)1.

[2] M. Ishi, Nucl. Instr. and Meth., 127(1975)53.

[3] C. C. Kuo, Design of Mini-Orange Spectrometers and their Application to Nuclear Structure Studies. Ph.D. Thesis, U. of Pittsburgh, 1986.

[4] J. X. Saladin, O. Dietzsch, C. Y. Chen, I. Y. Lee, C. Baktash, N. Johnson and M. Halbert, Bull. Am. Phys. Soc. 31(1986)1212.

[5] M. P. Metlay, J. X. Saladin, I. Y. Lee and O. Dietzsch, Nucl. Instr. and Methods in Phys. Res., A336(1993)162.

[6] T. Dresel, W. Elze and R. Peckhaus, Nucl. Instr. and Meth. in Phys. Res., A275(1989)301.

[7] T. Dresel, W. Elze and R. Peckhaus, Nucl. Instr. and Meth. in Phys. Res., A297(1990)441.

[8] W. Newmann, L. Cleemann, J. Eberth, N. Wiehl and V. Zobel, Nucl. Instr. and Meth., 164(1979)539.

[9] H. R. Faust, Nucl. Instr. and Meth., 213(1983)277.

[10] J. van Klinken, W. Z. Venema and V. A. Wichers, Nucl. Instr. and Meth. in Phys. Res., A286(1990)202.

[11] J. van Klinken, S. J. Feenstra, K. Wisshak, H. Faust, Nucl. Instr. and Meth., 130(1975)427.

[12] J. van Klinken, S. J. Feenstra, G. Dumont, Nucl. Instr. and Meth., 151(1978)433.

[13] J. R. Reitz, F. J. Milford, R. W. Christy, Fundamentals of the Electromagnetic Theory. Addison-Wesley, 1979.

[14] Y. Wu and T. P. Armstrong, Nucl. Instr. and Meth. in Phys. Res., A265(1988)561.

[15] W. H. Press, B. P. Flannery, S. A. Teukolsky and W. T. Vetterling, Numerical Recipes, Cambridge University Press, 1986.

[16] V. A. Kuzminikh and S. A. Vorobiev, Nucl.Instr. and Meth. 129(1975)561.

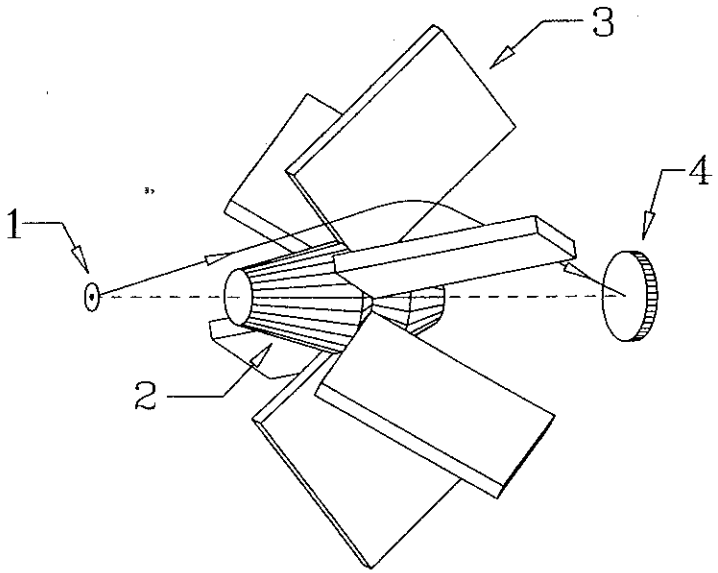

Figure 1

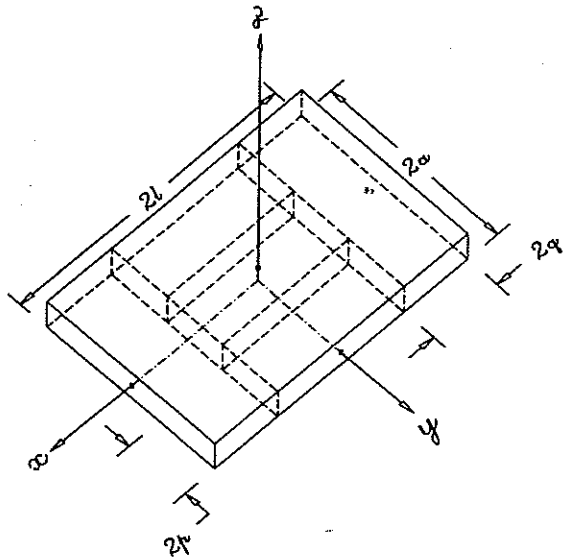

Figure 2

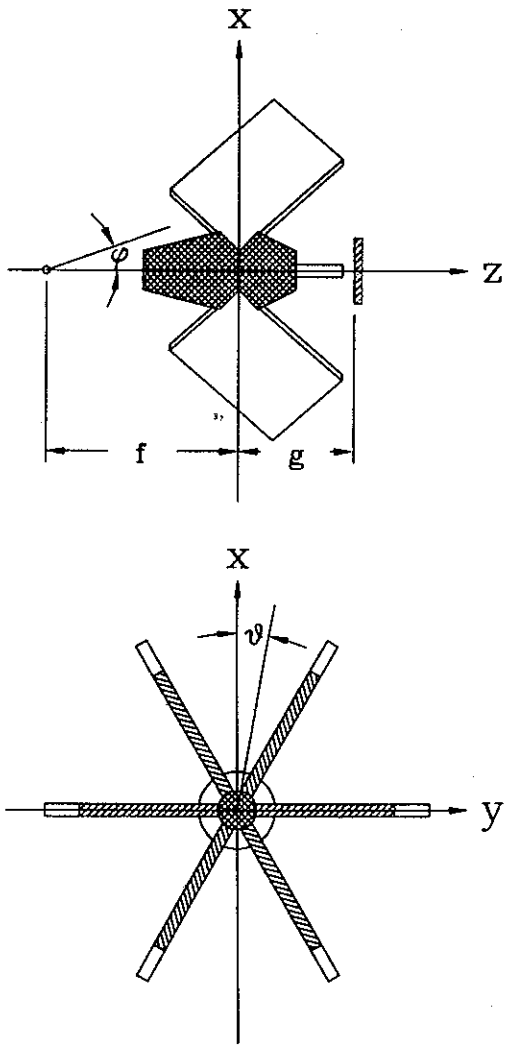

Figure 3

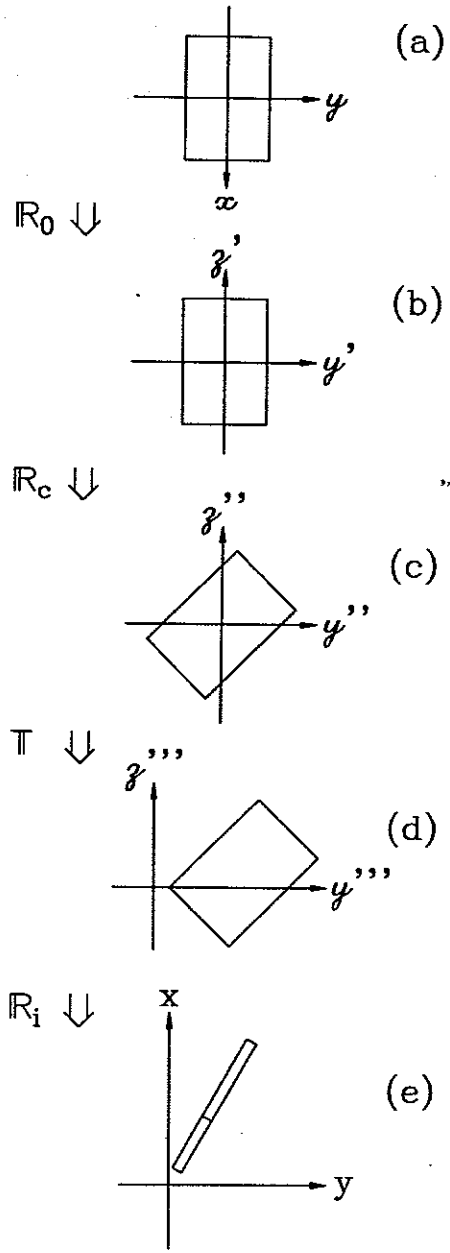

Figure 4

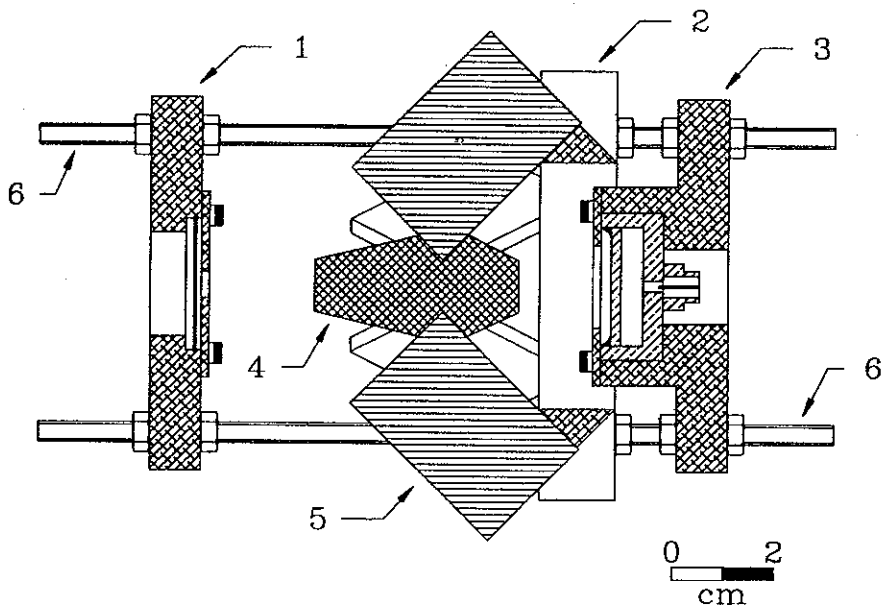

Figure 5

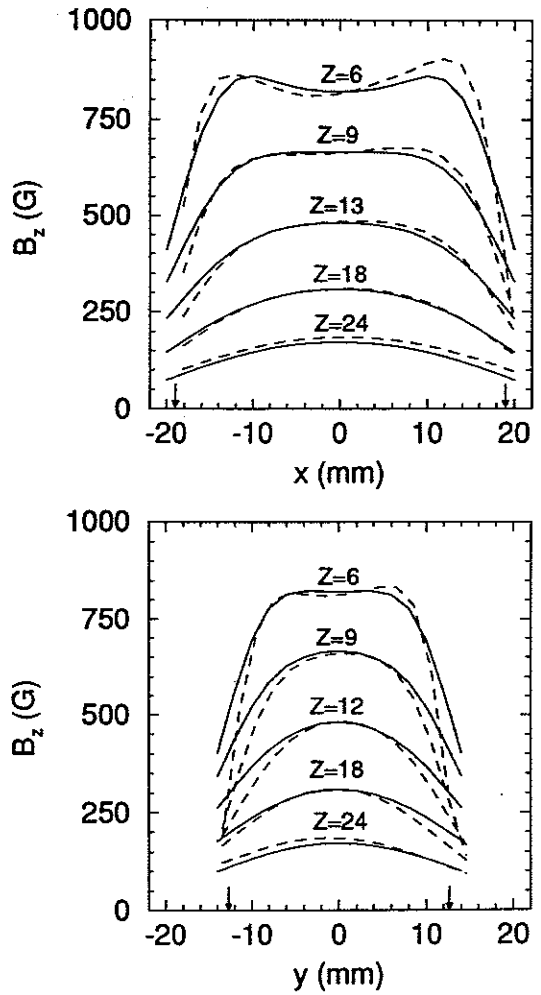

Figure 6

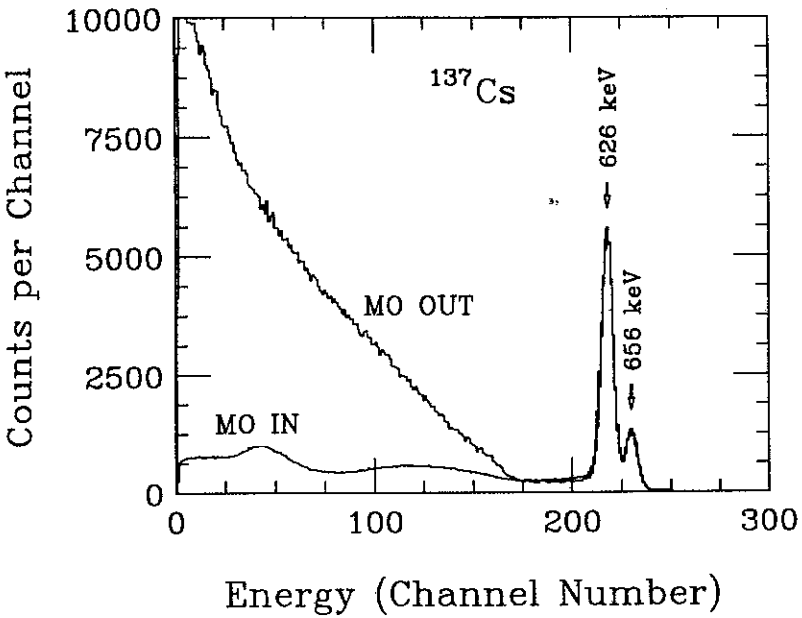

Figure 7

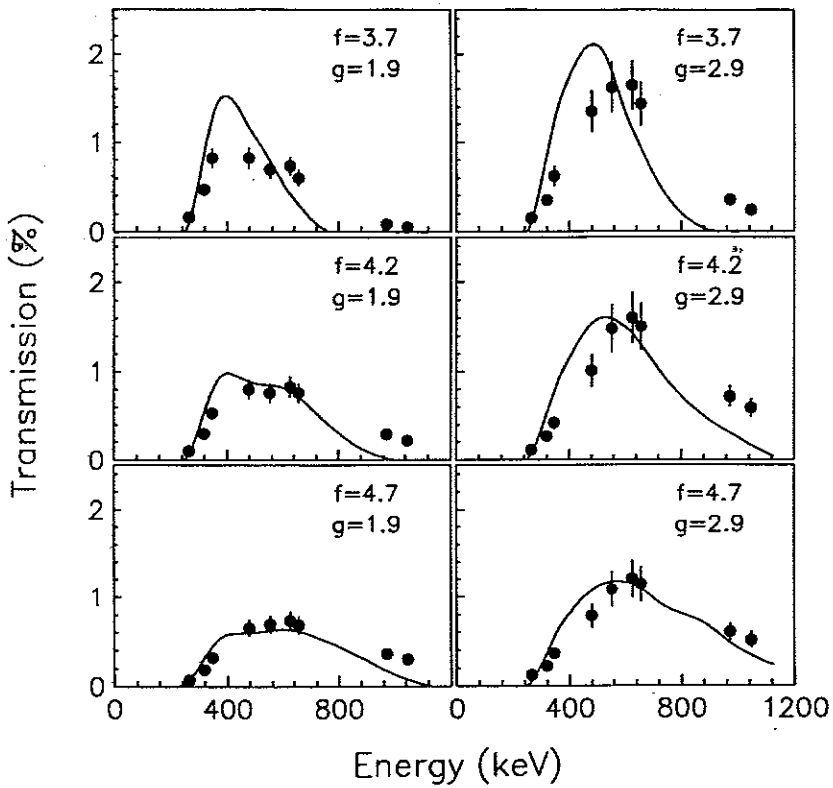

Figure 8

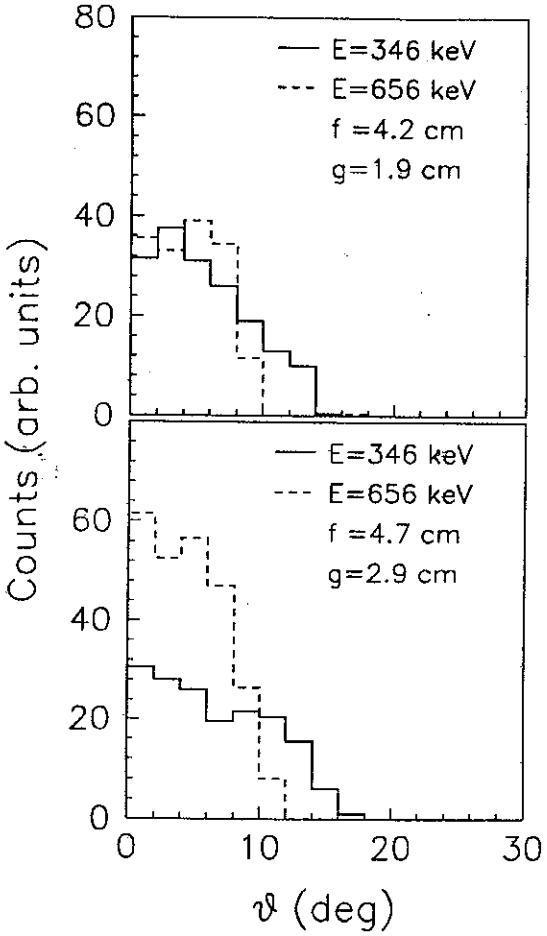

Figure 9

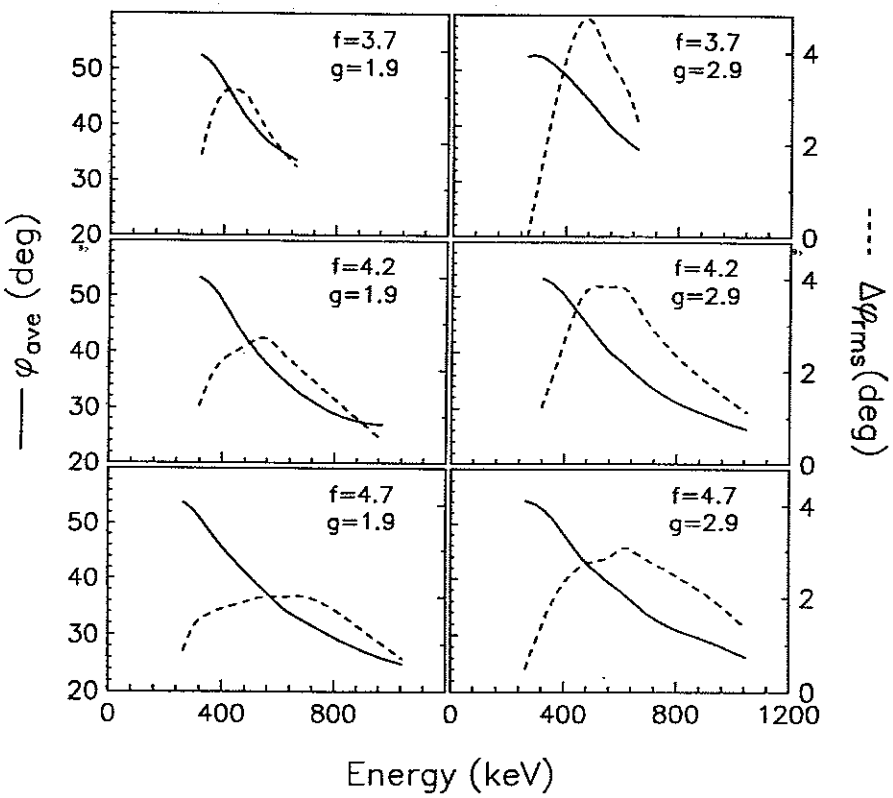

Figure 10